THE ASTROPHYSICAL JOURNAL, 532:467–473, 2000 March 20

INTERFEROMETRIC OBSERVATIONS OF IRC +10011 AND IRC +10420 IN THE MID-INFRARED

E. A. LIPMAN,[1] D. D. S. HALE, J. D. MONNIER, P. G. TUTHILL, W. C. DANCHI, AND C. H. TOWNES
Space Sciences Laboratory and Department of Physics, University of California at Berkeley, Berkeley, CA 94720; lipman@helix.nih.gov
Received 1999 August 15; accepted 1999 November 8

ABSTRACT

The 11 μm fringe visibilities of IRC +10011 (= CIT3) and IRC +10420 have been measured at baselines ranging from 2 to 14 m with a two-telescope interferometer. The visibility data provide one-dimensional profiles of these two stars and their immediate surroundings with higher resolution in this spectral range than is presently possible with a single-aperture telescope. Spherically symmetric radiative transfer models suggest that IRC +10011 is surrounded by a dust shell with an inner radius subtending 0".033, which falls off in density as $r^{-1.5}$, slightly slower than the r^{-2} expected for constant dust outflow. IRC +10420 appears to have a dust shell of inner radius 0".12, the density of which drops very slowly compared with that in a constant outflow. This implies decreasing outflow or a significant emission in the past.

Subject headings: circumstellar matter — infrared: stars — stars: AGB and post-AGB — stars: individual (IRC +10011, IRC +10420) — techniques: interferometric

1. INTRODUCTION

Evolved stars and their dust shells are attractive targets for observation using mid-infrared interferometry. Fringe visibility curves obtained in this region of the spectrum yield spatial information, unavailable by any other means, about relatively cool circumstellar material. Previous studies of this type (see, e.g., Sutton et al. 1978; Cobb & Fix 1987; Dyck & Benson 1992; Danchi et al. 1994) have provided valuable insight into the form and characteristics of the matter ejected by giant stars. The collection of such information on a wide range of sources promises to further increase our understanding of mass loss and the late stages of stellar evolution.

The recent addition of near-infrared guiding and tip-tilt correction systems (Lipman et al. 1998) to the University of California, Berkeley Infrared Spatial Interferometer (ISI) (Hale et al. 2000) has enabled the observation of sources with little visible flux. We have measured the fringe visibilities of two such objects, IRC +10011 and IRC +10420, at 11 μm. The resulting data, in conjunction with infrared spectra, have been used to construct radiative transfer models of the sources and their surroundings.

1.1. *IRC +10011*

IRC +10011 (= CIT3) is an oxygen-rich long-period variable star of spectral type M9. It has a K-band magnitude of 2.0 and a flux density at 11 μm of 1200 Jy,[2] making it an ideal candidate for study by the ISI. Some properties of IRC +10011 (and IRC +10420) are shown in Table 1. This source exhibits maser emission on both SiO (Cho et al. 1998) and OH lines. Outward flow of material from the star causes the OH maser emission to have a double-peaked spectrum, with a redshifted component caused by the receding material on the far side and a blueshifted component from the approaching material on the near side. As the luminosity of the star varies, the masers on either side of the star vary synchronously in intensity. As seen from Earth, however, the intensity variations in the redshifted and blueshifted components are out of phase because of the time required for light to travel from the far side of the star. By measuring this phase lag, Jewell et al. (1980) determined the linear diameter of the OH emission region around IRC +10011 to be $(6.6 \pm 1.4) \times 10^{16}$ cm.

Using the linear OH shell diameter in combination with their angular diameter data from the Very Large Array, Bowers et al. (1983) found a distance of 500 pc to IRC +10011. This distance was adopted for the modeling of ISI data. Although the stated uncertainty in the measurement was a factor of 2, it agrees with other estimates, such as that from a period-luminosity relation (650 pc, as given by Le Bertre & Winters 1998). CO line emission observations (Knapp & Morris 1985) indicate an outflow velocity of 23.0 ± 0.9 km s^{-1} for circumstellar material. Based on the work of Perrin et al. (1998) and the spectral type M9, the effective temperature for modeling of IRC +10011 was taken to be 2700 K.

The variation in luminosity of IRC +10011 can be seen in its mid-infrared spectra, taken at various times over a three yr period (Monnier et al. 1998). The luminosity cycle has a period of 660 days (Le Bertre 1993). ISI measurements during 1997 spanned a range of phases between 0.59 and 0.76 cycles, where the maximum luminosity occurs at a phase of 1 (or 0). Within a few years, enough ISI data should be available to see how the visibility curve for this source changes with the star's luminosity. In addition to the substantial change in overall mid-infrared flux during a cycle, there is also a noticeable variation in the shape of the silicate feature just below 10 μm (see Fig. 1). This feature is seen in absorption, indicating an optical depth greater than 1 (compare with the spectrum of IRC +10420 in Fig. 2, which shows the feature in emission). The characteristics of these spectra are discussed in detail by Monnier et al. (1998).

A measurement of the diameter of IRC +10011 at three infrared wavelengths was done in the early 1970s (Zappala et al. 1974) using lunar occultation. The results were modeled with a combination of two uniform disks. The best-fit model at 10 μm consisted of an outer disk with angular radius 0".068 producing 85% of the observed flux

[1] Present address: Laboratory of Chemical Physics, Building 5, Room 114, National Institutes of Health, Bethesda, MD 20892-0520.

[2] By comparison, the flux from α Orionis is approximately 4600 Jy at 11 μm.

TABLE 1

PROPERTIES OF IRC +10011 AND IRC +10420

Property	IRC +10011	IRC +10420	Reference
Right Ascension (2000.0)	1 6 25.92	19 26 48.00	1
Declination (2000.0).....	+12 35 53.2	+11 21 16.6	1
V-band Magnitude	>20	11	2, 3
K-band Magnitude	2.2[a]	3.4	2, 3
11 μm Flux Density (Jy)[b].....	1350[c]	1500	4
Spectral Type	M9.5–M10.0	F8–A5[d]	5, 6
Effective Temperature (K).....	2700	7000	7, 8
Distance (pc).....	500	5000	9, 3

NOTE.—Units of right ascension are hours, minutes, and seconds, and units of declination are degrees, arcminutes, and arcseconds.

[a] Measured at a luminosity phase $\phi = 0.82$ (see Fig. 1 and legend).

[b] 1 Jansky (Jy) = 10^{-26}W · m^{-2} · Hz^{-1}.

[c] Measured at $\phi = 0.65$.

[d] The spectral type of IRC +10420 has changed over the past 20 yr.

REFERENCES.—(1) CDS SIMBAD 1998; (2) Zappala et al. 1974; (3) Jones et al. 1993; (4) Monnier et al. 1998; (5) Lockwood 1985; (6) Klochkova et al. 1997; (7) Perrin et al. 1998; (8) Oudmaijer et al. 1996; (9) Bowers et al. 1983.

and an inner disk of radius 0.″033 contributing the remaining 15%. The authors also concluded that not more than 15% of the flux originated from a region more than 0.″2 from the center of the source. Recent measurements by Sudol et al. (1999) suggest that no significant mid-infrared flux originates beyond 0.″6 from the star. The fraction of power contained in extended dust emission led Zappala et al. to suggest that the optical depth of the shell at 10 μm was between 1 and 3.

1.2. *IRC +10420*

IRC +10420 is a luminous supergiant that has been extensively studied over the past 25 yr. Like IRC +10011, it is oxygen-rich; however, the two objects differ in a number of respects. As is illustrated by the unchanging flux levels in its mid-infrared spectra (Monnier et al. 1998), IRC +10420 does not exhibit significant periodic luminosity variations. In addition, it has a much earlier spectral type than IRC +10011. The initial measurement (Humphreys et al. 1973) yielded a spectral type of F8 Ia. Recent observations Oudmaijer (1998) indicate that the spectral type is now much earlier and that the effective temperature of IRC +10420 increased by 1000–2000 K between 1973 and 1994. Klochkova et al. (1997) find a spectral type of A5 based on recent data. Dramatic changes in the OH maser emission over the same time period have been reported by Nedoluha & Bowers (1992).

IRC +10420 is often characterized as "peculiar" (Diamond et al. 1983; Oudmaijer et al. 1996). This source is indeed unusual in that it is the only known OH maser source with spectral type earlier than K (Lewis et al. 1986), and its maser spectrum does not exhibit the common double-peaked velocity signature at 1612 MHz from stellar outflow (Bowers 1984). In addition, the 9.7 μm silicate feature (Fig. 2) is seen in emission in the spectrum of IRC +10420. OH maser sources are frequently surrounded by optically thick dust shells and show this feature in absorption.

Maser emission from this star has been studied by a number of authors. Based on his analysis of 1612 and 1667 MHz data, Bowers (1984) concluded that there has been "extensive mass loss" within about the last 500 yr and that the distribution of material around the star is in a "clumpy" sphere. Diamond et al. (1983) found that their 1612 MHz observations, taken at roughly the same time, could best be explained with a bipolar outflow model. Later results by Nedoluha & Bowers (1992) still indicated evidence for clumps of emitting material, despite changes in maser intensity and angular distribution.

In 1993, Jones et al. presented a review of a number of different observations of IRC +10420, including optical and infrared spectra, imaging, photometry, and polarimetric data. In their paper, a strong case is made for a distance of between 4000 and 6000 pc to IRC +10420 based on interstellar reddening and polarization in addition to observations of sodium D lines in the spectrum. Furthermore, this estimate is consistent with the kinematic distance and implies an intrinsic luminosity of $5 \times 10^5\ L_\odot$, which is normal for such a supergiant. For ISI modeling, a distance of 5000 pc was chosen, along with an effective temperature of 7000 K based on the work of Oudmaijer et al. (1996). Jones et al. combined their results in a model that consists of a central star surrounded by an equatorial disk that is tilted with respect to our line of sight. Recent imaging work by this group (Humphreys et al. 1997), using the *Hubble Space Telescope* and a 3.6 m ground-based infrared telescope, shows complex structure surrounding the star, including jets, arcs, and condensations. Their infrared images display bipolar emission along a northeast-southwest axis in a 4″ × 4″ field of view.

Other imaging work has been done on IRC +10420. Early near-infrared speckle interferometry (Dyck et al. 1984) indicated the presence of a dust shell that has approximately the same size along north-south and east-west baselines at a given wavelength (The FWHM of a Gaussian fit to the shell was 0.″072 at 2.2 μm and 0.″154 at 4.8 μm.) Ridgway et al. (1986) modeled near-infrared speckle measurements and found an inner radius of 0.″125 ± 0.″015 for a spherical dust shell. Cobb & Fix (1987) published visibility curves from 10 μm speckle interferometry on IRC +10420 and concluded that in the north-south and east-west directions the source is symmetric to within their experimental errors. Direct imaging has been done by Bloemhof et al. (1989) using a scanned linear array of 10 μm detectors and a 3 m telescope. They found a FWHM of 0.″36 for a Gaussian fit to the dust shell. Polarimetric imaging in the near-

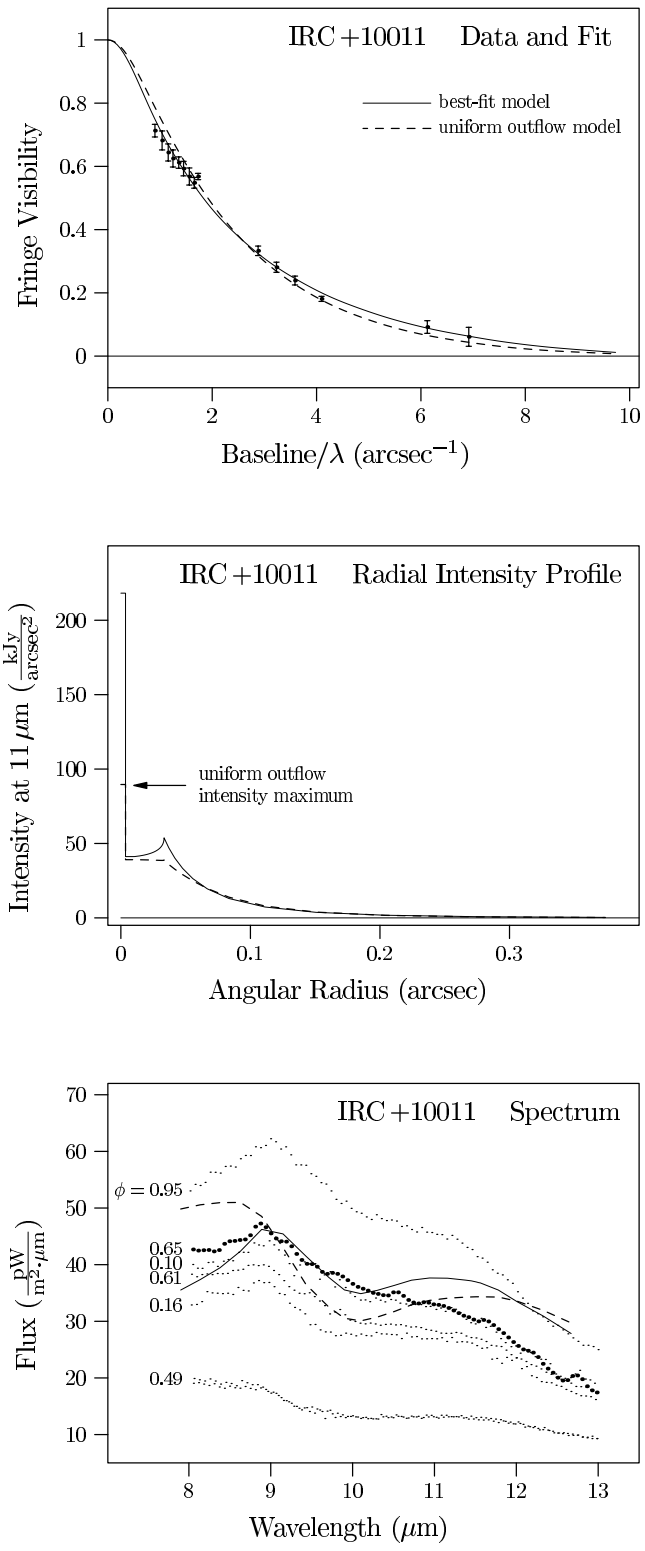

FIG. 1.—IRC +10011 fringe visibility data and radiative transfer models. The 11 μm fringe visibility data are shown at the top with visibility curves generated from the two models. Model parameters are given in Table 5. Radial intensity profiles corresponding to the visibility curves are given in the middle graph. The spectral energy distributions from Monnier et al. (1998) are shown in the bottom plot, along with those generated by the models. The highlighted spectrum (*bold dots*), which was used in the modeling, was taken when IRC +10011 was at a luminosity phase $\phi = 0.65$, closest to the average phase ($\phi = 0.67$) during the ISI observations. Luminosity phases (in cycles) are indicated next to the spectra, with maximum luminosity occurring at $\phi = 1$ (or 0). The spectra were acquired between 1994 August 26 and 1997 August 29. Two separate spectra, taken 660 days apart, are shown for $\phi = 0.49$.

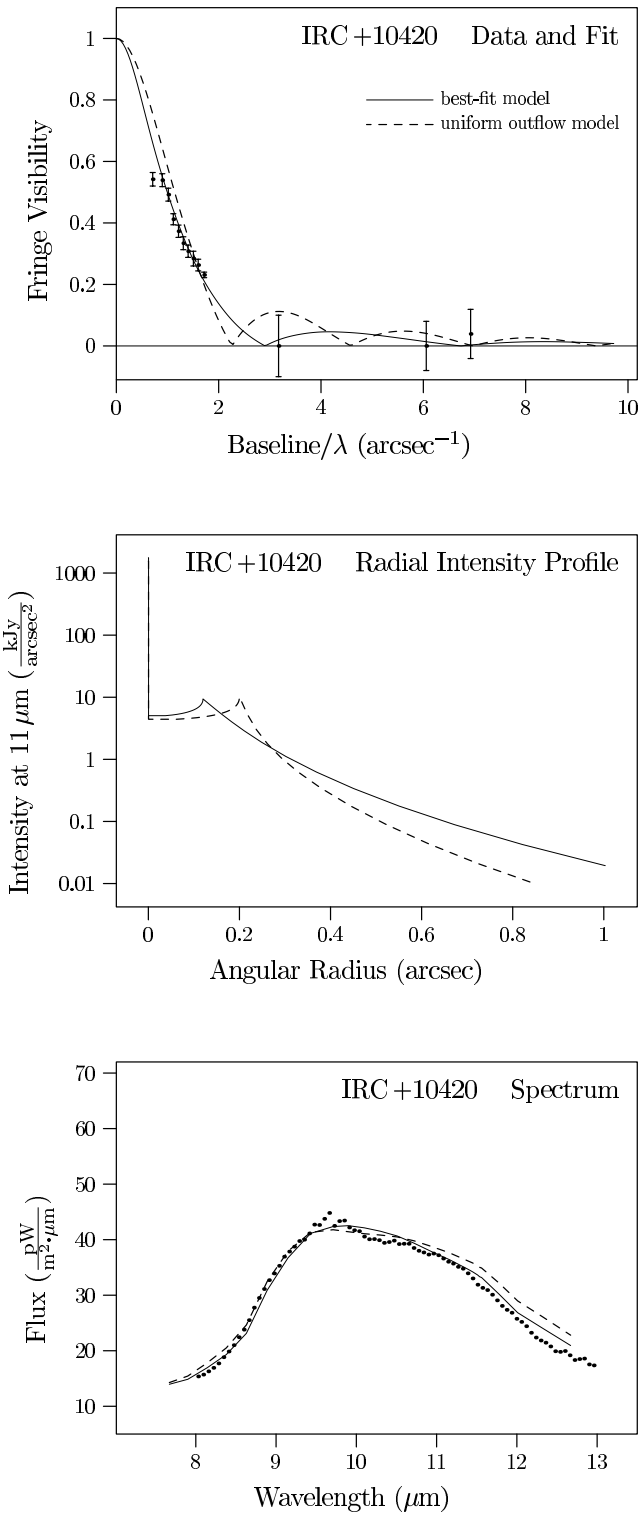

FIG. 2.—IRC +10420 fringe visibility data and radiative transfer models. Model parameters are given in Table 6. The data point at the shortest baseline was not used in the modeling (see § 2.2). IRC +10420 does not exhibit significant periodic luminosity variations, so a spectrum (*bold dots*) from Monnier et al. (1998) was chosen based on the fact that it was taken on 1997 August 28— during the period of ISI observations. Note the logarithmic scale used for the radial intensity profile.

infrared (Kastner & Weintraub 1995) revealed roughly circularly symmetric emission out to 9″.

2. 11 μm VISIBILITY MEASUREMENTS

11 μm visibility data were collected with the University of California, Berkeley Infrared Spatial Interferometer on a total of 21 nights for IRC +10011, and 18 nights for IRC +10420, between 1997 August 12 and 1997 December 10. The ISI, a two-element heterodyne interferometer using movable Pfund telescopes, is described elsewhere (Hale et al. 2000). Calibration of the visibility measurements was done by comparison with measurements of α Tauri. With its angular diameter of approximately 0.″02 and no significant dust shell, α Tau approximates a point source over the range of baselines used by the ISI during the 1997 observing season. An extensive discussion of the guiding system that made measurement of these sources possible, as well as the ISI fringe detection system, calibration, and data reduction procedures, has been given by Lipman (1998).[3] Three baselines were used for both sources, 4.0 m prior to October 5, 16.0 m from October 5 until November 6, and 9.6 m for the rest of the season. Table 2 shows the position angles of the effective baselines for the measurements. Although spherical symmetry was assumed for all 11 μm modeling purposes, the position angles are needed when making comparisons with measurements that have two-dimensional coverage.

2.1. *IRC +10011*

1997 fringe visibility data for IRC +10011 are shown at the top left of Figure 1 and in Table 3. Uncertainties given for the visibility data are 1σ values based on the scatter of the individual fringe visibility measurements that have been averaged (in groups of between 4 and 30) to give the visibility for each effective baseline. Some measurements of this source were also taken at the end of the 1996 season on the 4 m baseline. Although the quality of the 1996 data was extremely poor (uncertainty in the fringe visibility was approximately 0.25) because the new guiding system had not yet been optimized, the results were consistent with the 1997 values. The visibility curve shows a gradual but steady drop out to the longest measured baseline. This drop indicates the presence of a dust shell with an extent on the order of 0.″1.

2.2. *IRC +10420*

The measured visibility curve for IRC +10420 is shown in Figure 2 and Table 4. This curve can be seen to drop off very rapidly, and by the time the spatial frequency reaches 3 arcsec^{-1}, there is little or no power left to be resolved. This indicates that the mid-infrared emission comes from an extended region around the star and that the fraction of power received from the central point, which corresponds to the star itself, is comparatively insignificant.

A small amount of data was acquired on IRC +10420 during the 1994 observing season by guiding the telescopes manually. At the time, the interferometer was at its maximum available baseline of 32 m. The fringe visibility at this long baseline, if not zero, was very small. The measured visibility value was 0.1; however, the uncertainty was large enough that the measurement was consistent with a value of 0.

The point at the shortest effective baseline, 0.71 arcsec^{-1}, was not used during the modeling of IRC +10420. A systematic drop in visibility was seen at the shortest effective baselines for many sources during the 1997 season (Lipman 1998), probably caused by poor atmospheric conditions near the horizon or the intrusion of one of the ISI mirrors into the other's field of view. It should be noted that the discarded point is a near-perfect match to the value measured by Sudol et al. (1999) at this baseline. Although it is

TABLE 2

POSITION ANGLES FOR 11 μM OBSERVATIONS OF IRC +10011 AND IRC +10420

	Position Angle[a] (°)	
Baseline (m)	IRC +10011	IRC +10420
4.0	260–297	240–274
9.6	296–307	297–303
16.0	303–315	303–308

[a] The position angle ϕ_p is defined such that if the effective baseline vector points to the north, $\phi_p = 0°$, and if it points east, $\phi_p = 90°$.

[3] Lipman, E. A. 1998, Ph.D. thesis, University of California at Berkeley, is also available at http://isi.ssl.berkeley.edu/.

TABLE 3

11 μM FRINGE VISIBILITY VALUES FOR IRC +10011

Baseline/λ (arcsec^{-1})	Fringe Visibility
0.90	0.713 ± 0.020
1.04	0.682 ± 0.030
1.16	0.644 ± 0.027
1.25	0.625 ± 0.027
1.36	0.612 ± 0.018
1.45	0.593 ± 0.023
1.56	0.568 ± 0.027
1.66	0.548 ± 0.017
1.73	0.568 ± 0.010
2.88	0.333 ± 0.015
3.23	0.281 ± 0.016
3.59	0.239 ± 0.014
4.10	0.181 ± 0.008
6.12	0.092 ± 0.020
6.92	0.061 ± 0.030

TABLE 4

11 μM FRINGE VISIBILITY VALUES FOR IRC +10420

Baseline/λ (arcsec^{-1})	Fringe Visibility
0.71	0.542 ± 0.022
0.90	0.539 ± 0.021
1.02	0.492 ± 0.021
1.11	0.412 ± 0.018
1.21	0.373 ± 0.020
1.31	0.334 ± 0.021
1.40	0.308 ± 0.020
1.51	0.284 ± 0.024
1.60	0.263 ± 0.019
1.72	0.231 ± 0.009
3.17	0.0 ± 0.10
6.06	0.0 ± 0.080
6.92	0.039 ± 0.080

likely that there is a discrepancy in calibration between the ISI data and the measurement of Sudol et al. (1999), it is possible that there is a short stretch of almost constant fringe visibility at this point.

3. RADIATIVE TRANSFER MODELING

The modeling of ISI data has been described extensively by Danchi et al. (1994). A summary of the procedure, along with a discussion of selected parameters, will be presented here. The radiative transfer code is adapted from one developed by Wolfire & Cassinelli (1986) for studying accretion flows. The model consists of a star, taken to be an ideal blackbody at the specified temperature $T_\star$, and a spherically symmetric dust shell. The assumption of spherical symmetry is necessary because of the limited range of baseline orientations used in the observations (see Table 2). The dust is assumed to be composed of silicates, based on the prominent 9.7 μm feature in the mid-infrared spectra of the observed objects.[4] Various other properties of the dust, such as the size distribution, optical characteristics, and relative density compared with that of circumstellar gas, are taken from studies of the interstellar medium (Mathis et al. 1977) and measurements of circumstellar silicate opacities (Ossenkopf et al. 1992 and references therein). The dust is assumed to be fully condensed at the inner radius $r_{\rm inner}$, and the combined density of the gas and dust falls off according to a specified power law ($\rho \propto r^{-\ell}$). The density $\rho_{\rm outer}$ is specified at $r_{\rm outer}$ to set the scale for ρ, which, in turn, determines the total optical depth τ. The choice of $r_{\rm outer}$ is arbitrary, so long as it is beyond the edge of the ISI beam.

Given the physical model of the star and its surroundings, the radiative transfer code computes a self-consistent radial temperature profile using an iterative procedure. From this profile and the optical properties of the dust shell, the code produces a mid-infrared spectrum and radial brightness profile. The brightness profile is multiplied by the telescope beam pattern and processed using a fast Hankel transform algorithm (Hansen 1985) to yield a model visibility curve, which can be compared with ISI data. The computed temperature $T_{\rm inner}$ at the inner radius of the dust shell is given for each model in Tables 5 and 6.

The process of finding the best model parameters is as follows. First, the distance to the star and effective temperature are chosen. The distance D sets the length scales in the model, since only the angular extent of the star is indicated by the data. The models are, however, not very sensitive to this parameter, and the model chosen for IRC +10011 was essentially unaffected by a 40% change in D. The effective temperature $T_\star$ is selected to match the spectral type of the star. The modeling is also not very sensitive to $T_\star$, since $r_\star$ can be changed to vary the total amount of flux from the source.

TABLE 5

IRC +10011 MODEL PARAMETERS

Parameter	Best-fit Model	Uniform Outflow Model
χ^2	33	44
τ	1.75	2.95
D (pc)	500	500
$T_\star$ (K)	2700	2700
$r_\star$ (arcsec)	0.0036	0.0036
$r_{\rm inner}$ (arcsec)	0.033	0.033
$T_{\rm inner}$ (K)	998	1030
ρ	$\propto r^{-1.5}$	$\propto r^{-2}$

[4] The code is also capable of including graphites and two phases of amorphous carbon if appropriate.

TABLE 6

IRC +10420 MODEL PARAMETERS

Parameter	Best-fit Model	Uniform Outflow Model
χ^2	12	120
τ	0.635	0.762
D (pc)	5000	5000
$T_\star$ (K)	7000	7000
$r_\star$ (arcsec)	0.00043	0.00039
$r_{\rm inner}$ (arcsec)	0.12	0.20
$T_{\rm inner}$ (K)	674	480
ρ	$\propto r^{-0.5}$	$\propto r^{-2}$

Once D and $T_\star$ have been chosen, typical values are assigned to $r_{\rm inner}$ and $\rho_{\rm outer}$, and ℓ is set to be 2, which corresponds to the density profile for a constant outflow from the star. The stellar radius $r_\star$ is then varied in order to match the total flux in the model spectrum with that in a measured spectrum, such as those from Monnier et al. (1998).

At this point, $r_{\rm inner}$ and $\rho_{\rm outer}$ are varied to produce the best possible fits to the mid-infrared spectrum and the visibility curve. If satisfactory fits cannot be obtained, ℓ is changed and the procedure is repeated.

Each time the model is run, two values are computed that facilitate the comparison between the model and the data. The agreement between a model and the measured visibility curve can be characterized by the parameter (Bevington 1969)

$$\chi^2 \equiv \sum_{i=1}^{N} \frac{[y_i - f(x_i)]^2}{\sigma_i^2},$$

where y_i are the N visibility values at spatial frequencies x_i, σ_i are the uncertainties in y_i, and $f(x)$ is the visibility curve generated by the model. Although χ^2 provides a convenient measure of the quality of the fit, it should not be regarded as an absolute indicator of this quality. For ISI data, χ^2 tends to emphasize the fit at short baselines, since the data are denser there.

The optical depth τ of the dust shell is determined primarily by $\rho_{\rm outer}$ and ℓ, which together specify the amount of dust between the star and the observer. There is also an effect on τ when $r_{\rm inner}$ is changed, since the highest density of dust is at $r_{\rm inner}$. The shape of the mid-infrared spectrum is strongly influenced by the optical depth. Whether the dust shell is optically thick (opaque) with $\tau > 1$ or optically thin (transparent to some degree) will determine if spectral features, such as the 9.7 μm silicate peak, will be seen in absorption or emission and to what extent. The constraint placed on τ by the spectral data provides a useful check of the assumption of spherical symmetry. If the visibility curve cannot be fit well under conditions that match the spectrum, it may indicate that the source is actually surrounded by a disk or other more complicated dust distribution instead of a spherical shell.

3.1. *IRC +10011*

The spherical-shell radiative transfer models for IRC +10011 are shown in Figure 1, and the parameters are given in Table 5.

The best-fit model has a central star with angular radius $r_\star = 0\farcs0036$, which, at $D = 500$ pc, corresponds to a linear distance of about 390 solar radii. This is large, but reasonable for an asymptotic giant. The inner radius of the dust shell is $0\farcs033$, or about $9r_\star$. The temperature, $T_{\rm inner}$, of the dust at the inner radius for this model is somewhat lower than the 1300 K which is typical for dust condensation. A 10% increase in $r_{\rm inner}$ for this model results in a 3% increase in χ^2 and a 5% drop in the optical depth. A 10% increase in $\rho_{\rm outer}$ produces a 44% increase in χ^2 and a 10% increase in τ.

A good match to the curve implied by the visibility data could only be obtained using a dust shell density, approximately proportional to $r^{-1.5}$, which falls off slower than the r^{-2} which would result from constant, uniform dust outflow. The best uniform outflow model is also shown in Figure 1. This model produced a much higher optical depth ($\tau = 2.95$ as opposed to $\tau = 1.75$ in the best-fit model), and consequently the fit to the spectrum was considerably worse.

A number of factors could be responsible for the poor fit of the spectrum from the best model (Fig. 1) at wavelengths beyond 10 μm. First, data on IRC +10011 were taken over a range of luminosity phases between $\phi = 0.59$ and $\phi = 0.76$. At the bottom left of Figure 1, it can be seen that the shape of the spectrum changes with luminosity phase. The spectrum chosen for comparison with the model is simply that at an average phase and does not take into account the amounts of data taken at any particular phase nor whether various parts of the spectrum change at different rates. Second, Monnier et al. (1998) suggest that dust properties may change during the luminosity cycle. Such a change would not be accounted for in the ISI radiative transfer model, which assumes constant optical properties and location (distance from the star) of formation for the dust grains. Finally, the assumption of spherical symmetry may be incorrect.

3.2. *IRC +10420*

The models for IRC +10420 are shown in Figure 2, and the parameters for these models are given in Table 6. Even though the central star is extremely bright compared to the dust shell, far more power is delivered by the shell because of its enormous extent. The stellar radius $r_\star$ in the best-fit model was taken to be $0\farcs00043$, which corresponds to 460 solar radii. Because of the high temperature of IRC +10420, the region where it is cool enough for dust to condense lies far from the photosphere. The dust shell inner radius is thus much larger than for IRC +10011 at $280r_\star$. In addition, the low value of $T_{\rm inner}$ indicates that the inner boundary of the dust shell has traveled outward since condensing. For this model, an increase of 10% in $r_{\rm inner}$ results in a 230% increase in χ^2 and a 1% decrease in τ. An increase of 10% in $\rho_{\rm outer}$ produces a 30% increase in χ^2 and a 10% increase in τ.

Although the best-fit model for IRC +10420 matched very well with the fringe visibility and spectral data, it was necessary to use a radial density profile proportional to $r^{-0.5}$, which is substantially different from that resulting from constant dust outflow. Figure 2 also shows the best model that was possible assuming uniform outflow. It is clearly inferior. Thus, we can infer that either the assumption of spherical symmetry is incorrect or the production of circumstellar dust has decreased over time.

4. DISCUSSION OF RESULTS

4.1. *IRC +10011*

The model fits to data on IRC +10011 produce a picture of the star and its surroundings in good agreement with other available observations. As predicted by Sudol et al. (1999), the angular radius beyond which there is no measurable emission is well within $0\farcs6$. The inner dust shell radius of $0\farcs033$ corresponds to that of the inner disk chosen by Zappala et al. (1974) to model their lunar occultation data. As was pointed out by Ridgway et al. (1986) and Ivezić & Elitzur (1996), the inner radius should not be wavelength dependent. As yet unpublished measurements by our group using aperture masking on the Keck telescope (technique described by Tuthill et al. 1998) find no ellipticity or other substantial deviations from axial symmetry in the near-infrared image of the source. This lends credence to the assumption of spherical symmetry, although it is still possible that the dust shell is actually a disk seen pole-on from the Earth.

The 11 μm model optical depth $\tau = 1.75$ yields a good fit to the silicate feature of the spectrum at a phase that matches the average during ISI observations. It is consistent with the prediction of Zappala et al. that the 10 μm optical depth should lie between 1 and 3. Monnier et al. (1998) also predict that τ for IRC +10011 should be "only slightly smaller than that of NML Cyg," which has an optical depth of about 2.

A number of radiative transfer models have been done for IRC +10011 (Justtanont et al. 1994; Le Sidaner & Le Bertre 1996). By assuming uniform, spherically symmetric mass outflow and using a mass-loss rate inferred from infrared spectra, Justtanont et al. (1994) derived a radial temperature profile for the source. Although the general shape of the profile approximates that resulting from the ISI model, the overall level of the ISI profile is substantially higher because Justtanont et al. adopted an effective temperature of 2000 K for IRC +10011. Their infrared modeling (Justtanont & Tielens 1992) did, however, produce values for $r_\star$ and $r_{\rm inner}$ within 50% of those in the ISI model, which is not unreasonably far off, considering the assumptions used in the modeling, such as a somewhat arbitrary luminosity of $10^4\ L_\odot$ and constant dust outflow. The lack of measured parameters in these models frustrates attempts at meaningful quantitative comparison with ISI data.

The mass density $\rho \propto r^{-1.5}$ implies that there is more dust farther from the star than would be expected from a constant dust outflow. This has been the case in other ISI models, such as those for IRC +10216 (Danchi et al. 1994). Two possible explanations for the slow drop in density are time-varying dust emission and deviation from spherical symmetry. If dust was produced at a greater rate in the recent past, there will be a region of relatively high density moving away from the star. It is possible, assuming a dust condensation temperature of 1300 K and an original shell with similar parameters to that in the model, to calculate the time at which dust condensation ceased. Using an outflow velocity of 23 km s^{-1} (Knapp & Morris 1985) and $T_{\rm inner}$ from the best-fit model, one finds that the shell around

IRC +10011 has apparently been traveling outward with no new dust formation for approximately 1.5 yr. Circumstellar dust in some form other than a spherical shell, for example a disk or some sort of lobe structure, could also cause the model density to mimic a time-varying outflow. Additional interferometric measurements at a variety of wavelengths should shed more light on the form of the material around this and other evolved stars.

4.2. *IRC +10420*

The ISI visibility curve for IRC +10420 can be compared at the shortest baselines with the mid-infrared speckle data of Cobb & Fix (1987). At a spatial frequency of 0.9 arcsec^{-1}, the ISI fringe visibility is 15% lower than that measured by Cobb & Fix. This could indicate miscalibration of the ISI data, although there is also a possibility that the value from the speckle data is too high. That measurement seemed to have a systematic problem that resulted in rapidly rising visibility values at spatial frequencies greater than 1 arcsec^{-1}.

The ISI radiative transfer model compares well with other available measurements. The overall size of the radial profile in Figure 2 matches fairly well with the size of the Gaussian model given by Bloemhof et al. (1989), and the inner radius $r_{\rm inner} = 0\farcs12$, which should not be wavelength dependent (Ridgway et al. 1986; Ivezić & Elitzur 1996), matches almost perfectly with that derived by Ridgway et al. (1986). The optical depth $\tau = 0.635$ provides an excellent fit to the mid-infrared spectrum with the silicate feature in emission.

That the dust shell density in the IRC +10420 radiative transfer model is radically different from that produced by constant outflow deserves consideration. The model power law $\rho \propto r^{-0.5}$ requires that there be a large amount of dust far from the inner radius. Humphreys et al. (1997) point out that the silicate feature and large fraction of extended emission in the mid-infrared argue against a constant outflow. Mutel et al. (1979) suggested that the dust shell surrounding IRC +10420 might be a remnant from an earlier stage in the star's evolution. Based on a spectroscopically measured outflow velocity, Bloemhof et al. (1989) estimated that the dust emission occurred on the order of 100 yr ago. Nedoluha & Bowers (1992) interpret their data as possibly supporting the hypothesis of a large emission during a previous epoch, and Humphreys et al. conclude, using an outflow velocity derived from measurements of CO lines, that the dust within 1″ of the star was ejected within the last 600 yr. This is consistent with the maser observations discussed in § 1.2. A calculation (see § 4.1) using $T_{\rm inner}$ from the best-fit ISI model, assuming a 1300 K dust condensation temperature and a 40 km s^{-1} (Oudmaijer et al. 1996) outflow velocity, gives 55 yr since the last new dust formation. A relatively recent dust emission event thus seems to be a likely explanation for the density profile in the ISI model.

The explanation of the model density profile must also take into consideration the assumption of spherical symmetry. Although a number of the measurements mentioned in § 1.2 suggest that the source is fairly close to being axially symmetric, images collected by Humphreys et al. (1997) show much complex structure, as well as bipolar mid-infrared emission oriented in such a fashion that north-south and east-west baselines could measure the same dust shell size, even though the shell is not circular. If the dust around IRC +10420 is in the form of a disk, a bipolar outflow, or clumps, this could certainly affect the model parameters. Future ISI observations with two-dimensional coverage should eliminate this ambiguity and provide a complete picture of the circumstellar environment.

The authors would like to thank Manfred Bester, Walter Fitelson, and Michael Johnson for their helpful discussions and substantial contributions to the ISI. We would also like to thank Terry McDonald for his skillful fabrication of parts for the interferometer. The authors made extensive use of the NASA ADS abstract service and the CDS SIMBAD database during the course of this research. Financial support was provided by the National Science Foundation (grants AST-9315485, AST-9321289, and AST-9500525) and the Office of Naval Research (grants N00014-93-0775, N00014-96-0737, and N00014-97-1-0743).

REFERENCES

Bevington, P. R. 1969, Data Reduction and Error Analysis for the Physical Sciences (New York: McGraw-Hill)
Bloemhof, E. E., Danchi, W. C., & Townes, C. H. 1989, in ASP Conf. Proc. 9, Sixth Cambridge Workshop on Cool Stars, Stellar Systems, and the Sun, ed. G. Wallerstein (San Francisco: ASP), 463
Bowers, P. F. 1984, ApJ, 279, 350
Bowers, P. F., Johnston, K. J., & Spencer, J. H. 1983, ApJ, 274, 733
Cho, S.-H., Chung, H.-S., Kim, H.-R., Oh, B.-Y., Lee, C.-H., & Han, S.-T. 1998, ApJS, 115, 277
Cobb, M. L., & Fix, J. D. 1987, ApJ, 315, 325
Danchi, W. C., Bester, M., Degiacomi, C. G., Greenhill, L. J., & Townes, C. H. 1994, AJ, 107, 1469
Diamond, P. J., Norris, R. P., & Booth, R. S. 1983, A&A, 124, L4
Dyck, H. M., & Benson, J. A. 1992, AJ, 104, 377
Dyck, H. M., Zuckerman, B., Leinert, C., & Beckwith, S. 1984, ApJ, 287, 801
Hale, D. D. S., et al. 2000, ApJ, in press
Hansen, E. W. 1985, IEEE Trans. Acoustics, Speech, and Signal Processing, ASSP-33, 666
Humphreys, R. M., et al. 1997, AJ, 114, 2778
Humphreys, R. M., Strecker, D. W., Urdock, T. L., & Low, F. J. 1973, ApJ, 179, L49
Ivezić, Z., & Elitzur, M. 1996, MNRAS, 279, 1011
Jewell, P., Webber, J., & Snyder, L. 1980, ApJ, 242, L29
Jones, T. J., et al. 1993, ApJ, 411, 323
Justtanont, K., Skinner, C. J., & Tielens, A. G. G. M. 1994, ApJ, 435, 852
Justtanont, K., & Tielens, A. G. G. M. 1992, ApJ, 389, 400
Kastner, J. H., & Weintraub, D. A. 1995, ApJ, 452, 833
Klochkova, V. G., Chentsov, E. L., & Panchuk, V. E. 1997, MNRAS, 292, 19
Knapp, G. R., & Morris, M. 1985, ApJ, 292, 640
Le Bertre, T. 1993, A&AS, 97, 729
Le Bertre, T. & Winters, J. M. 1998, A&A, 334, 173
Le Sidaner, P., & Le Bertre, T. 1996, A&A, 314, 896
Lewis, B. M., Terzian, Y., & Eder, J. 1986, ApJ, 302, L23
Lipman, E. A. 1998, Ph.D. thesis, University of California at Berkeley
Lipman, E. A., Bester, M., Danchi, W. C., & Townes, C. H. 1998, Proc. SPIE, 3350, 933
Lockwood, G. W. 1985, ApJS, 58, 167
Mathis, J. S., Rumpl, W., & Nordsieck, K. H. 1977, ApJ, 217, 425
Monnier, J. D., Geballe, T. R., & Danchi, W. C. 1998, ApJ, 502, 833
Mutel, R. L., Fix, J. D., Benson, J. M., & Webber, J. C. 1979, ApJ, 228, 771
Nedoluha, G. E., & Bowers, P. F. 1992, ApJ, 392, 249
Ossenkopf, V., Henning, T., & Mathis, J. S. 1992, A&A, 261, 567
Oudmaijer, R. D. 1998, A&AS, 129, 541
Oudmaijer, R. D., Groenewegen, M. A. T., Matthews, H. E., Blommaert, J. A. D. L., & Sahu, K. C. 1996, MNRAS, 280, 1062
Perrin, G., Foresto, V. C. d., Ridgway, S. T., Mariotti, J. M., Traub, W. A., Carleton, N. P., & Lacasse, M. G. 1998, A&A, 331, 619
Ridgway, S. T., Joyce, R. R., Connors, D., Pipher, J. L., & Dainty, C. 1986, ApJ, 302, 662
Sudol, J. J., Dyck, H. M., Stencel, R. E., Klebe, D. I., & Creech-Eakman, M. J. 1999, AJ, 117, 1609
Sutton, E. C., Storey, J. W. V., Townes, C. H., & Spears, D. L. 1978, ApJ, 224, L123
Tuthill, P. G., Monnier, J. D., Danchi, W. C. & Haniff, C. A. 1998, Proc. SPIE, 3350, 839
Wolfire, M. G., & Cassinelli, J. P. 1986, ApJ, 310, 207
Zappala, R. R., Becklin, E. E., Matthews, K., & Neugebauer, G. 1974, ApJ, 192, 109